International Journal of Solids and Structures 51 (2014) 416–429

Contents lists available at ScienceDirect

International Journal of Solids and Structures

journal homepage: www.elsevier.com/locate/ijsolstr

Thermo-elastic optimization of material distribution of functionally graded structures by an isogeometrical approach

A.H. Taheri [a], B. Hassani [a,*], N.Z. Moghaddam [b]

[a] Mechanical Engineering Department, Ferdowsi University of Mashhad, P.O. Box 91775-1111, Mashhad, Iran
[b] Civil Engineering Institute, Technical and Vocational University of Mashhad (Shahid M. Montazeri), P.O. Box 9176994594, Mashhad, Iran

ARTICLE INFO

Article history:
Received 6 July 2013
Received in revised form 22 September 2013
Available online 24 October 2013

Keywords:
Isogeometric
Material design
Thermo-elasticity
Functionally graded materials
Volume fraction

ABSTRACT

A new isogeometrical procedure for optimization of material composition of functionally graded structures in thermo-mechanical processes is introduced. The proposed method employs a generalized form of the standard isogeometric analysis method, allowing for gradation of material properties through patches. The variations of material properties are captured in a fully isogeometric formulation using the same NURBS basis functions employed for construction of the geometry and approximation of the solution. Subsequently, the applicates of control points that define the surfaces of volume fractions of the constituents are considered as the design variables and obtained by solving the optimization problem using a mathematical programming algorithm. Some numerical examples under thermal and mechanical loadings are considered to demonstrate the performance and applicability of the proposed method. Comparison of the obtained results with those of the other existing approaches such as finite elements and meshfree methods verifies the presented results. It will be seen that the proposed procedure considerably removes the difficulties of the existing methods and provides a promising tool for material design of functionally graded structures.

1. Introduction

Functionally graded materials (FGMs) are considered as one of the modern generation of composite materials. These materials are commonly two-phase particulate composites, e.g. ceramic and metallic alloy phases, microscopically engineered to have a smooth spatial variation of material properties in order to improve the overall performance. This is accomplished by fabricating the composite material to have a gradual variation in the relative volume fractions of the constituent phases and microstructure. FGMs are ideal candidates for applications involving severe thermal gradients, ranging from thermal structures in advanced aircraft and aerospace engines to computer circuit boards (Shiota and Miyamoto, 1997). It is important to note that the performance of FGMs is not merely a function of the properties and relative amounts of their material constituents, but is also directly related to the ability of the designer to utilize the materials in the most optimal fashion (Goupee and Vel, 2007). Accordingly, the optimization of material distribution is a fundamental step in the design of FG components, which demands the accurate simulation of its response to applied complex thermo-mechanical loadings.

1.1. Techniques of analysis and optimization of FGMs

With FGMs being used mainly for thermal barrier coatings, many studies have focused on thermo-mechanical behavior of these materials under thermal or combined thermo-mechanical loads. For instance, Lü et al. (2006) presented a two-dimensional (2D) thermo-elasticity solution for functionally graded thick beams. Ding et al. (2007) derived an elasticity solution for plane anisotropic FG beams with elastic compliance parameters being arbitrary functions of the thickness coordinate. A semi-analytical elasticity solution for bending and thermal deformations of bi-directional FG beams was introduced by Lü et al. (2008). Also, many researchers investigated thermal fracture of functionally graded plates and shells under thermal loadings or thermal shocks (Feng and Jin, 2009; Guo and Noda, 2010; Guo et al., 2008; Sheng and Wang, 2011; Ueda, 2001). Since, in general, it is not simple to obtain an analytical solution to the partial differential equations with variable coefficients governing to thermo-mechanical response of FGMs, we are usually obliged to resort to numerical methods.

By now, different numerical techniques such as finite difference, finite elements and meshfree methods have been employed for their thermo-mechanical analysis. For instance, Ching and Yen (2005) employed the meshless local Petrov–Galerkin (MLPG) method for the analysis of 2D FG elastic solids under mechanical

* Corresponding author. Tel.: +98 9121732312; fax: +98 5118763304.
E-mail addresses: b_hassani@um.ac.ir, behrooz.hassani@gmail.com (B. Hassani).

0020-7683/$ - see front matter © 2013 Elsevier Ltd. All rights reserved.
http://dx.doi.org/10.1016/j.ijsolstr.2013.10.014

and thermal loads. Wang and Qin (2008) developed a meshless algorithm to simulate the static thermal stress distribution in 2D FGMs on the basis of analog equation theory and the method of fundamental solutions coupling with radial basis functions. Also, Chareonsuk and Vessakosol (2011) investigated numerical solutions for functionally graded solids under thermal and mechanical loads using a high-order control volume finite element method.

On the other hand, lots of strategies have been proposed for the optimization of material distribution of FGMs, thus far. Cho and Ha (2002a) deals with the volume fraction optimization for minimizing steady-state thermal stresses in Ni–Al_2O_3 heat-resisting FGM composites where the interior penalty-function and golden section methods are employed as optimization techniques. He also employs the finite difference method for sensitivity analysis and an appropriate material-property estimate for calculating thermo-mechanical properties of the graded layer. Cho and Ha (2002b) address a 2D volume fraction optimization procedure for relaxing the effective thermal stress distribution by using bilinear finite elements for the approximation of volume fraction field. Turteltaub (2002) deals with the control and/or optimization of a two-phase isotropic composite under time-dependent thermo-mechanical loadings. The research concludes that for the minimum structural compliance problem, the optimal distribution of material properties depends on the loading history, even though the deformations are elastic.

In one of the most related numerical works, Goupee and Vel (2006b) investigate the application of the element-free Galerkin method for optimization of material composition of two phase metal-ceramic FGMs in thermo-elasticity problems. The spatial distribution of ceramic volume fraction is obtained by piecewise bicubic interpolation of volume fractions defined at a finite number of grid points. Subsequently a real-coded genetic algorithm is adopted to minimize the peak thermal stress or mass of FG structures. Optimization of volume fractions for functionally graded plates and panels considering stress and critical temperature is investigated in Na and Kim (2009a,b, 2010). Nemat-Alla (2009) discussed reduction of thermal stresses by composition optimization of 2D FGMs assuming analytical power law functions for variations of volume fractions of the constituents. Optimization of material composition of FGMs based on multiscale thermo-elastic analysis for thermal stress relaxation was conducted by Chiba and Sugano (2012). In the presented method, location-dependent unit cells representing the microstructures of two-phase FGMs are created using morphology description functions, and the homogenized material properties and microscale thermal stresses are computed using the asymptotic expansion homogenization method. Recently, Kou et al. (2012) have presented a procedural model for optimal design of FGMs using the particle swarm optimization method. In this work, instead of using the widely used explicit functional models, a feature tree based model is proposed to represent generic material heterogeneities. A procedural model of this sort allows more than one explicit function to be incorporated to describe versatile material gradations and so the material composition at a given location is no longer computed by simple evaluation of an analytic function, but obtained by execution of customizable procedures (Kou et al., 2012). Surendranath et al. (2003) proposed a methodology to enhance the optimization of material distributions in composite structures using gradient architectures. It is demonstrated that genetic algorithms (GAs) can be enhanced for composite structures by constraining the design search space through a reduction in the number of design variables thereby the computational effort is substantially reduced. Some researchers deal with thermo-elastic optimization of FGMs with temperature dependent material properties (Bobaru, 2007; Boussaa, 2009; Goupee and Vel, 2007). Simultaneous optimization of material properties and topology of FG structures was also undertaken in many researches (Almeida et al., 2010; Paulino and Silva, 2005; Xia and Wang, 2008).

It needs to be mentioned that, a developed optimization method for material design of FGMs requires some significant characteristics to be considered as an efficient one. First, the ability of the method in creating complex material profiles using least possible numbers of design variables is definitely of primary importance. This makes the procedure to become computationally more efficient. Next, the smoothness of the obtained optimal material profiles that do not contain discontinuities or jumps throughout the domain is very desirable which can also facilitate their fabrication (Goupee and Vel, 2006a,b). It is evident that the smoothness of the optimal material profile is directly related to the order of continuity and differentiability of the employed material profile. However, considering the literature, one can see that most of reported strategies for material design and optimization of FGMs suffer from major difficulties in these senses.

Regarding the employed design parameterization scheme, we can classify the reported approaches into two main classes of functional models and discrete models. Functional models employ typical analytical functions for description of material gradation through the computational domain so that some coefficients of the functions are selected as the design variables for optimization of the material distribution. It is evident that adopting such a methodology, despite being computationally efficient as well as having higher order of continuity and ease of implementation, lacks the primary advantage of creating complicated material profiles.

On the other hand, discrete models which are more commonly adopted, partition the domain of interest into a collection of subdomains wherein the material properties are either assumed homogeneous or are interpolated. Due to the fact that these models naturally use a larger number of design variables, they are more capable to produce complex material distributions. However, most of them suffer from drawbacks of impossibility of having any desirable order of material distribution continuity throughout the domain as well as demanding a large number of design variables for creation of complex material profiles which makes them computationally inefficient.

A commonly used nodal based approach is the so-called continuous approximation of material distribution (CAMD) technique (Kumar and Gossard, 1996; Matsui and Terada, 2004) which employs the shape functions within the elements and subsequently throughout the design domain to obtain the densities for layout and topology optimization (Almeida et al., 2010). The main idea of this concept was initially introduced by Kim and Paulino (2002) as the generalized graded finite elements for the analysis of heterogeneous materials.

It is a well-known fact that the use of higher-order finite elements for approximation of material distributions is effective against checker-board patterns and results in clearer topologies (Matsui and Terada, 2004). However, we note that higher order shape functions are not always positive within an element. This means that the approximated value of the design variable by these shape functions can be negative locally in an element and violate the geometrical constraint for the design variable, i.e. $0 \leqslant \rho(\mathbf{x}) \leqslant 1$, even if the nodal design variables are all positive (Matsui and Terada, 2004). Hence, most of researchers have employed linear shape functions for capturing the material gradations inside elements in the graded finite element context in optimization problems, even though the solution is approximated by higher order shape functions (Almeida et al., 2010; Cho and Ha, 2002b). For more details, the interested reader is referred to (Almeida et al., 2010; Matsui and Terada, 2004). It is evident that such a remedy reduces the order of continuity of the material description model and accordingly the smoothness and applicability of the obtained optimal material profile.

Bobaru (2007) also faced the same problem in employing shape preserving cubic splines for continuous volume fraction representation. The continuous volume fraction function profile that defines the FGM is approximated by an Akima spline controlled by a set of design variables. "While the oscillations of cubic spline interpolation are reduced in the Akima spline interpolation, some portions of the Akima spline may still exit the physical domain allowed for the volume fraction function: the interval $[0,1]$" (Bobaru, 2007). In order to preserve the curve in desired region, when the curve exits the allowable domain, instead of using the Akima splines a typical modified continuous function is employed, which consequently violates the order of continuity of the material profile. Similar limitations were encountered and reported by Almeida et al. (2010) and Paulino et al. (2008) in the introduction of a global–local approach to layout and material gradation in topology optimization of FG structures, and optimal design of periodic functionally graded composites with prescribed properties, respectively.

It should be noted that, by now lots of attempts have been done to circumvent this difficulty. For instance, Brodlie et al. (1995) addresses the problem of interpolation subject to simple linear constraints. Specifically, it looks at the problem of constructing a piecewise bicubic function $u(x,y)$ from data on a rectangular mesh, such that $u(x,y)$ is nonnegative (positive). They derive sufficient conditions for positivity in terms of the first partial derivatives and mixed partial derivatives at the grid points. Many researchers have adopted this technique to increase the continuity of their material profiles. Particularly, Goupee and Vel (2006a,b, 2007) adopt the range-restricted piecewise bicubic interpolation technique devised by Brodlie et al. (1995), to obtain a smooth volume fraction profile that is C^1 continuous everywhere when employing the meshfree methods for material distribution or topology optimization problems. In this technique, the volume fraction at an arbitrary point in the domain is obtained by interpolation of the volume fraction values defined at the grid points. The employed range-restricted interpolation ensures that the volume fractions lie strictly in the range of 0 to 1 at all points within the domain (Goupee and Vel, 2006b). In order to obtain C^1 continuity in the entire domain, they employ the Hermite basis functions, which demand the provision of the derivatives of material distribution functions on the employed grid points. The derivatives can be employed as extra design variables or estimated by numerical methods, that either way will increase the required computational effort.

1.2. Analysis and design of FGMs by the isogeometric method

As observed, despite existing different strategies for the analysis of FGMs, still serious difficulties arise when these strategies are employed for their material design and optimization. In order to circumvent these problems, in this paper, we investigate the applicability of the recently improved isogeometrical analysis method introduced by Hassani et al. (2013) for material distribution optimization of FGMs in thermo-elasticity problems.

It should be noted the developed approach which is introduced as an efficient tool for the stress analysis of functionally graded elasticity problems, takes inspiration from the work of Kim and Paulino (2002) and allows for gradation of material properties through patches. In analogy to the suggested procedure by Kim and Paulino (2002), called generalized isoparametric graded finite elements, we employ the graded patches wherein the material properties are interpolated at the Gauss points in a fully isogeometric concept using the same NURBS basis functions employed for construction of the geometry and approximation of the solution. Besides being an efficient approach for the analysis of heterogeneous problems, it will be seen that, this brings us about the possibility of creating any desired complex material profile as well as the accessibility of any desired order of continuity when employed as a tool for material design of FGMs. Owing to the possibility of simultaneously modeling of the structural shape and material distribution, the proposed generalized isogeometrical analysis (GIGA) approach constitutes a capable tool for studying integrated modeling, analysis and design of FGMs. It will be seen that the proposed method offers a great promise for material design of FGMs by exploiting the significant capabilities of NURBS basis functions. It should be noted that, recently a NURBS based finite element method is also proposed by Valizadeh et al. (2013) for static bending, vibration, buckling and flutter analysis of FG plates.

2. Surface creation by NURBS

Since in the proposed method, variations of the material properties are sought as imaginary NURBS surfaces over the computational domain, we here briefly review the surface definition by NURBS and the important properties of these surfaces. For more details the interested reader is referred to (Piegl and Tiller, 1997).

A NURBS surface is parametrically constructed as

$$\mathbf{S}(\xi,\eta)\sum_{i=0}^{n_1}\sum_{j=0}^{n_2}R_{ij}^{p,q}(\xi,\eta)\mathbf{P}_{ij} \tag{1}$$

where $\mathbf{P}_{ij}$ are a net of $(n_1+1)(n_2+1)$ control points and $R_{ij}^{p,q}$ are defined as

$$R_{ij}^{p,q}(\xi,\eta)=\frac{N_{i,p}(\xi)N_{j,q}(\eta)w_{ij}}{\sum_{k=0}^{n_1}\sum_{l=0}^{n_2}N_{k,p}(\xi)N_{l,q}(\eta)w_{kl}} \tag{2}$$

where w_{ij} are the associated weights to every control points and $N_{i,p}(\xi)$ and $N_{j,q}(\eta)$ are the normalized B-spline basis functions of degree p and q, defined on the knot vectors $\Xi=\{\xi_0,\xi_1,\ldots,\xi_{n_1+p}\}$ and $\mathbf{H}=\{\eta_0,\eta_1,\ldots,\eta_{n_2+q}\}$, successively.

B-splines and NURBS have plenty of important and beneficial properties which make them promising candidates to be employed as a tool for material distribution and topology optimization problems. We here outline some of their main properties which provided us the inspiration for exploiting them in this research.

Strong convex hull property

If $(\xi,\eta)\in[\xi_{i_0},\xi_{i_0+1})\times[\eta_{j_0},\eta_{j_0+1})$, then $\mathbf{S}(\xi,\eta)$ is in the convex hull of the control points $\mathbf{P}_{ij}$, $i_0-p\leqslant i\leqslant i_0$ and $j_0-q\leqslant j\leqslant j_0$. This follows from the properties of basis functions.

The continuity and differentiability

The continuity and differentiability of $\mathbf{S}(\xi,\eta)$ follow from that of the basis functions. In particular, $\mathbf{S}(\xi,\eta)$ is $p-k$ (or $q-k$) times differentiable in the ξ (or η) direction, at a ξ (or η) knot of multiplicity k. Also, all derivatives of $\mathbf{S}(\xi,\eta)$ exist inside a knot span, that is $\mathbf{S}(\xi,\eta)$ is C^∞ inside knot elements.

Planar approximation of control net

If triangulated, the control net forms a piecewise planar approximation to the surface. This approximation is improved by knot insertion or degree elevation. As a general rule, the lower the degree, the closer a NURBS surface follows its control net. In particular, if $p=q=1$ the surface coincides on its control net.

3. Heat conduction and thermo-elastic analysis of FGMs by GIGA

3.1. Governing equations

The flow of heat in solids is associated with temperature differences within the material. This process is governed by the well-known Fourier law of heat conduction, which is the constitutive relation between the heat flux vector **q** and the temperature gradient ∇T. This theory formulates a linear relationship that is given by

$$q_i = -k_{ij}T_{,j} \tag{3}$$

where k_{ij} is the thermal conductivity tensor. It can be shown that this tensor is symmetric, i.e. $k_{ij} = k_{ji}$. For the isotropic case $k_{ij} = k\delta_{ij}$, and thus

$$q_i = -kT_{,i} \tag{4}$$

where k is a material constant called the thermal conductivity.

We consider an elastic solid that is stress free at a uniform temperature T_0 when all external forces are zero. This stress-free state is referred to as the *reference state*, and T_0 is called the reference temperature.

We recall that the stress follows from the Duhamel–Neumann constitutive relation, which for the isotropic case is given as

$$\sigma_{ij} = \lambda e_{kk}\delta_{ij} + 2\mu e_{ij} - (3\lambda + 2\mu)\alpha(T - T_0)\delta_{ij} \tag{5}$$

where λ is the so-called Lame's constant and α is the coefficient of thermal expansion.

Now using the principle of conservation of energy and the above generalized Hook's law, and neglecting the coupling term in the energy equation, we establish the so-called uncoupled conduction equation

$$kT_{,ii} = \rho c\dot{T} - \rho h \tag{6}$$

where ρ is the mass density, c is the specific heat capacity at constant volume and h is the heat generation. For most of applications, we consider only uncoupled theory and normally with no sources ($h = 0$). Another simplification is to consider only steady state conditions, and for this case the conduction equation reduces to the following elliptic equation for the temperature distribution which is known as the Laplace equation:

$$T_{,ii} = \nabla^2 T = 0 \tag{7}$$

where $\nabla^2 = \frac{\partial^2}{\partial x^2} + \frac{\partial^2}{\partial y^2}$. The above equation is subjected to the Dirichlet, Newman, and Robin's boundary conditions of (8a)–(8c).

$$T = \overline{T} \quad \text{on } \Gamma_\theta \tag{8a}$$

$$-q_j n_j = \overline{q} \quad \text{on } \Gamma_q \tag{8b}$$

$$-q_j n_j + h(T - T_\infty) = 0 \quad \text{on } \Gamma_c \tag{8c}$$

For this case, the temperature field can be determined independent of the stress-field calculations. Once the temperature is obtained, the following general uncoupled thermo-elastic analysis procedures can then be employed to complete the problem solution.

We recall the strain–displacement and the equilibrium equations are:

$$\varepsilon_{ij} = \frac{1}{2}(u_{i,j} + u_{j,i}) \tag{9}$$

$$\sigma_{ij,j} + F_i = 0 \tag{10}$$

where σ_{ij} is the Cauchy stress tensor and F_i are the components of the body force. Eq. (10) is subjected to the Dirichlet and Newman boundary conditions of (11a) and (11b)

$$u_i = \overline{u}_i \quad \text{on } \Gamma_u \tag{11a}$$

$$\sigma_{ij}n_j = \overline{t}_i \quad \text{on } \Gamma_t \tag{11b}$$

Using relations (5) and (9), the equilibrium equations (10), in the absence of body forces, reduce to the Navier's relations in terms of displacements as follows:

$$\mu\nabla^2 u + \frac{E}{2(1-\nu)}\frac{\partial}{\partial x}\left(\frac{\partial u}{\partial x} + \frac{\partial v}{\partial x}\right) - \frac{E}{1-\nu}\alpha\frac{\partial T}{\partial x} = 0 \tag{12a}$$

$$\mu\nabla^2 v + \frac{E}{2(1-\nu)}\frac{\partial}{\partial y}\left(\frac{\partial u}{\partial x} + \frac{\partial v}{\partial x}\right) - \frac{E}{1-\nu}\alpha\frac{\partial T}{\partial y} = 0 \tag{12b}$$

for plane stress case, and

$$\mu\nabla^2 v + (\lambda+\mu)\frac{\partial}{\partial y}\left(\frac{\partial u}{\partial x} + \frac{\partial v}{\partial x}\right) - (3\lambda + 2\mu)\alpha\frac{\partial T}{\partial y} = 0 \tag{13a}$$

$$\mu\nabla^2 u + (\lambda+\mu)\frac{\partial}{\partial x}\left(\frac{\partial u}{\partial x} + \frac{\partial v}{\partial x}\right) - (3\lambda + 2\mu)\alpha\frac{\partial T}{\partial x} = 0 \tag{13b}$$

for plain strain case.

Reviewing isothermal plane elasticity theory, it is observed that the temperature effect is equivalent to adding an additional body force $-(3\lambda + 2\mu)\alpha\frac{\partial T}{\partial x}$ to Navier's equations of equilibrium and adding a traction term $(3\lambda + 2\mu)\alpha(T - T_0)n_i$ to the applied boundary tractions for plane strain state. A similar statement could be made about the plane stress theory, and in fact this concept can be generalized to three-dimensional theory.

3.2. Improved isogeometrical solution procedure

In isogeometric analysis, the geometry is constructed using the NURBS surfaces as

$$\mathbf{x}(\xi,\eta) \approx \sum_{i=0}^{n_1}\sum_{j=0}^{n_2} R_{ij}^{p,q}(\xi,\eta)\mathbf{x}_{ij} = \mathbf{RP} \tag{14}$$

In the same manner, displacements are approximated over a patch by using the same NURBS basis functions as follows

$$\mathbf{u}(\xi,\eta) \approx \sum_{i=0}^{n_1}\sum_{j=0}^{n_2} R_{ij}^{p,q}(\xi,\eta)\mathbf{u}_{ij} = \mathbf{Rd} \tag{15}$$

In above equations, **d** and **P** are the vectors of degrees of freedom and coordinates of control points, respectively. It should be noted that in IGA, the easiest way to set Dirichlet boundary conditions is to apply them to the control variables (Hughes et al., 2005). In case of homogeneous Dirichlet conditions, which is the only case encountered in this study, this results in exact pointwise satisfaction by just setting the control variables as zeros (Hughes et al., 2005). In case of nonhomogeneous boundary conditions, however, this approach may result in significant errors and so various alternative strategies have been proposed (Embar et al., 2010; Liu et al., 2010).

Now, constituting the weak forms of Eqs. (12) or (13) and following the conventional variational approach similar to the classical FEM, the equivalent algebraic form of these equations for patch p is obtained as:

$$\mathbf{K}^p\mathbf{d}^p = \mathbf{f}^p \tag{16}$$

where

$$\mathbf{K}^p = \int_{V_p} \mathbf{B}^T\mathbf{C}\mathbf{B}\,dV, \tag{17}$$

$$\mathbf{f}^p = -\int_{\Gamma_t} \mathbf{N}^T\bar{\mathbf{t}}\,d\Gamma - \int_{V_p} \mathbf{B}^T\mathbf{C}\varepsilon_0\,dV \tag{18}$$

in which V_p denotes the volume of patch p, $\mathbf{C}$ is the elasticity matrix and $\mathbf{B} = \mathbf{DR}$, where $\mathbf{D}$ is the differential operator matrix and is defined as

$$\mathbf{D} = \begin{bmatrix} \frac{\partial}{\partial x} & 0 & \frac{\partial}{\partial y} \\ 0 & \frac{\partial}{\partial y} & \frac{\partial}{\partial x} \end{bmatrix} \tag{19}$$

Also, $\boldsymbol{\varepsilon_0}$ is the initial strain which, assuming $\mathbf{m} = [1, 1, 0]^T$, is obtained using relations (20a) and (20b) for the special cases of plane stress and plane strain, respectively.

$$\boldsymbol{\varepsilon_0} = \alpha(T - T_0)\mathbf{m} \tag{20a}$$

$$\boldsymbol{\varepsilon_0} = (1 + \nu)\alpha(T - T_0)\mathbf{m} \tag{20b}$$

It is noted that the global system of equations for multiple patch geometries is easily obtained following a conventional assembly procedure similar to the FEM. Moreover, it needs to be mentioned that the elements of the elasticity matrix $\mathbf{C}$, in case of FGMs, are not constants anymore and are varying continuously through the domain according to a specific distribution function. As previously mentioned, in GIGA we state these variations in a fully isogeometrical formulation using the same NURBS basis functions employed for the geometric and computational models. Once the control variables of displacements are calculated, the strains are obtained as $\boldsymbol{\varepsilon} = \mathbf{Bd}$. Subsequently, the stresses are recovered using the Duhamel–Newman constitutive equation (5), that is written in a new matrix form as

$$\boldsymbol{\sigma} = \mathbf{C}(\mathbf{Bd} - \boldsymbol{\varepsilon_0}) \tag{21}$$

3.3. Volume fraction distribution by GIGA

According to previous explanations, in the generalized isogeometrical analysis approach, the variable coefficients of differential terms are considered as imaginary surfaces over the computational domain, which are constructed by NURBS. The primary idea to this purpose is to state the volume fraction distribution of the constituents in a fully isogeometrical formulation using the same NURBS basis functions employed for construction of the geometry and approximation of the solution as

$$\mathbf{V}(\xi, \eta) = \sum_{i=0}^{n_1}\sum_{j=0}^{n_2} R_{ij}^{p,q}(\xi, \eta)\mathbf{V}_{(i,j)}, \quad 0 \leqslant V \leqslant 1 \tag{22}$$

where $\mathbf{V}_{(i,j)}$ are the coordinates of control points that produce the volume fraction NURBS surface of each of the constituents. It should be noted that in GIGA, following the concept of isoparametric approximation, the same net of control points is employed for construction of differential coefficients functions as for the geometry and solution surfaces. Hence, in this concept the in-plane coordinates of control points in Eqs. (15) and (22) are the same as $\mathbf{x}_{ij}$ in (14).

However, this is not the only available approach to this purpose. Sometimes, we may encounter problems where the stress distribution is too complicated and demand employing a very fine mesh, while the corresponding optimal material distribution for a specific goal is not so complex. It is noted that, in such cases it may not seem efficient to use the same net of control points employed for the analysis also as the design variables. In such applications, we can describe the variations of material properties using a coarser mesh in order to decrease the computational effort.

The important point in this case is that we use the same parameterization of computational domain for both the geometric (computational) and the material model. This ensures having the same mapping from parametric space to physical space for both the computational and material models and so will provide us the possibility of calculation of variable material properties at the Gauss points by taking their parametric coordinates from the computational model. In this work, we only employ the generalized isogeometrical concept by employing the same NURBS basis functions and the same net of control points for geometric modeling as well as material design.

In order to devise the optimization problem employing GIGA, it suffices to select the heights (applicates) of control points of the constituents as the design variables. Accordingly, we can produce any complex desired profile of material gradations by determining these variables. As Eq. (22) shows, the volume fraction value at any arbitrary point of the domain is restricted to lie within the interval $[0, 1]$. Following the proposed methodology, this constraint is easily handled by directly restricting the design variables to lie within the mentioned interval, no matter what degree of basis functions is employed. This facility is resulted from the important strong convex hull property of NURBS surfaces mentioned in previous sections.

Therefore, any desired level of continuity of the material profile can be achieved by employing the appropriate order of basis functions. Undoubtedly, increasing the order of continuity of the material profile will evidently result in smoother material distributions which are also easier to fabricate. It is noted that employing higher order shape functions in other numerical methods such as graded FEM or meshless methods, besides arising the difficulty of restricting the volume fractions within the side constraints, does not necessarily increase the continuity of the material profile over the whole domain. For instance, by employing higher order Lagrangian shape functions in finite elements, the order of continuity of the solution and the material profile on element borders is always C^0, no matter what degree the shape functions are.

As observed, the proposed method circumvents the difficulties of existing methods and does not require applying any restriction or extra computations. It is noted that the proposed method can also be easily adopted in the FGM design problems consisted of three or more component phases. For instance, in a typical three-component FGM design problem, it suffices to select the applicates of control points of two of the constituents that define their distribution over the domain as the design variables to be determined. In this case, the side constraints of restricting the volume fractions to $[0, 1]$ are applied to the summations of each of the control points heights selected as the design variables. The distribution of the third component is easily obtained by knowing the fact that the summation of all the volume fractions at any point of the domain equals one. Also, the method can be easily extended to be employed in 3D elasticity problems.

Furthermore, since in this approach, variations of material properties are defined by NURBS surfaces which are considered as a powerful tool in creating complicated shapes and surfaces, very complex material profiles can be obtained by using a relatively small number of control points that makes it computationally efficient. Hence, it is expected to yield superior results in comparison with the other available numerical methods such as graded FEM or meshless methods when the same numbers of design variables are used.

3.4. Estimation of effective material properties

In FGMs the constituent phases, e.g. ceramic and metal particles, are of arbitrary shapes and mixed up in arbitrary dispersions. Therefore, prediction of their effective material properties at a point by knowing the volume fractions of the constituents is not generally this simple. Different strategies have been proposed for this purpose thus far each of them may work well for a typical problem depending on the fabrication process and shapes of the constituent particles. The primary approach is known as the linear rule of mixtures in which a material property at a point is

estimated by the volume weighted average of the properties of its constituents. Although this simple rule is accurate for a fiber reinforced composite that is aligned in the loading direction and deformed under iso-strain conditions, the reliability of this method has been known to be highly questionable, because it does not include the details on particles and dispersion layout as well as the interaction effect between the constituents (Cho and Ha, 2002a). Therefore, designers seek more accurate estimations for the Young's modulus and the thermal expansion coefficients that dominate the thermoelastic response of FGMs (Cho and Ha, 2002a).

Later, Tomota et al. (1976) proposed a modified rule of mixtures by refining the linear rule of mixtures for the Young's modulus which will be subsequently explained in details. Two other homogenization techniques, i.e. the Mori–Tanaka (Mori and Tanaka, 1973) and self-consistent (Hill, 1965) schemes, are also widely employed in the literature and are believed to yield promising estimations of the effective material properties in typical realistic problems.

According to the Mori–Tanaka method, the effective bulk modulus (K), and the effective shear modulus (μ) of a mixture of two constituents is given by (Mori and Tanaka, 1973)

$$\frac{K-K_c}{K_m-K_c}=\frac{V_m}{1+(1-V_m)[3(K_m-K_c)/(3K_c+4\mu_c)]} \tag{23}$$

$$\frac{\mu-\mu_c}{\mu_m-\mu_c}=\frac{V_m}{1+(1-V_m)(\mu_m-\mu_c)/[\mu_c+\mu_c(9K_c+8\mu_c)/6(K_c+2\mu_c)]} \tag{24}$$

where subscripts "m" and "c" stand for the constituent phases, e.g. metal and ceramic. Subsequently, the effective Young's modulus (E) and Poisson's ratio (v) are obtained as $E=9K\mu/(3K+\mu)$ and $v=(3K-2\mu)/(6K+2\mu)$, respectively. In addition, the effective thermal conductivity (k) and coefficient of thermal expansion (α) are evaluated according to (25) and (26).

$$\frac{k-k_c}{k_m-k_c}=\frac{V_m}{1+(1-V_m)(k_m-k_c)/3k_c} \tag{25}$$

$$\frac{\alpha-\alpha_c}{\alpha_m-\alpha_c}=\frac{1/K-1/K_c}{1/K_m-1/K_c} \tag{26}$$

In this research, we will employ the modified rule of mixtures whose details will be elaborated later, as well as the Mori–Tanaka scheme for estimation of the effective material properties in the presented numerical experiments.

Furthermore, it should be noted that, in general, mechanical properties of materials are temperature dependent. However, variations of material properties with temperature are not usually remarkable and can be ignored if the thermal gradients are not too severe. The effect of temperature-dependent material properties is investigated in many researches and the interested reader is referred to Bobaru (2007), Boussaa (2009), Goupee and Vel (2007), and Na and Kim (2009b). In this study we assume the mechanical properties of the constituents to be temperature-independent.

4. Volume fraction optimization by mathematical programming

4.1. Formulation of the optimization problem

A classical constrained optimization problem is stated as follows

$$\begin{aligned}&\text{Minimize } f(\mathbf{S})\\&\text{Subject to: } g_k(\mathbf{S})\leqslant 0,\quad k=1,\ldots,n\end{aligned} \tag{27}$$

where $f(\mathbf{S})$ is the objective function, $\mathbf{S}$ is the vector of design variables, and g_k is the kth inequality constraint. It is noted that if there are any equality constraints, they are not usually explicitly stated in the optimization problem formulation and are easily handled by converting them into inequality constraints (Goupee and Vel, 2006a).

According to previous explanations, for the optimization problem under study, the elements of the vector of design variables in Eq. (27) are the third coordinates (applicates) of $\mathbf{V}_{(i,j)}$ which are here denoted by $V_c^{(i,j)}$ or $V_m^{(i,j)}$ for the ceramic or metal constituent phases. In thermo-elasticity problems, the objective functions are commonly considered as the peak effective stress or mass of the structure. Also, the applied constraints are usually set as these parameters or sometimes the maximum temperature experienced by the FGM components. The effective stress is defined as

$$\overline{\sigma}=\sqrt{\frac{3}{2}\tilde{\sigma}_{ij}\tilde{\sigma}_{ji}} \tag{28}$$

where $\tilde{\boldsymbol{\sigma}}$ is the deviatoric stress tensor and defined as

$$\tilde{\boldsymbol{\sigma}}=\boldsymbol{\sigma}-\frac{1}{3}[trace(\boldsymbol{\sigma})]\mathbf{I} \tag{29}$$

4.2. Mathematical programming

The optimization problem (27) can be solved through different available optimization algorithms. In this study, we employ the mathematical programming algorithms to this end. A large number of mathematical programming (MP) techniques such as linear or nonlinear programming algorithms exist. They provide a very general framework for scarce resource allocation and the basic algorithms originate in the operations research community (Vanderplaats, 1999).

In the present study, we concentrate on the application of the sequential quadratic programming (SQP) algorithm for the solution of the optimization problems. However, any other optimization algorithm can also be easily adopted in the same manner. We employ the design optimization tool (DOT) for implementation of MP algorithms to solve the optimization problems (Vanderplaats, 1999). The details of the concept of employed optimization algorithm are investigated in many researches. The interested reader can refer to Sinha (2005), Spillers and Macbain (2009), and references therein.

4.3. Sensitivity analysis

Whereas the mentioned algorithms are so-called "gradient based", calculations of sensitivities are required for specification of the search direction. Sensitivities can either be calculated numerically, semi-analytically or analytically. The most common numerical method for calculating gradients is the finite difference method which is also employed in this research. These sensitivities are calculated intrinsically by DOT. The employed design optimization tool has the ability of calculation of sensitivities using both first forward and central difference methods. Although central difference yields more accurate results, it almost doubles the computational effort. The first forward difference technique is employed in this research for this purpose. It is noted that for a mildly nonlinear optimization problem, such as the problems under study in this research, finite difference usually yields reasonable estimation of sensitivities. The primary advantage of this method, which has made it popular in engineering designs, is that if structural analysis can be performed and the performance measure can be obtained, then the gradients are virtually acquired independent of the problem types considered (Choi and Kim, 2004). However, high computational cost is the main disadvantage of this method

which makes it infeasible to be used for large-scale problems having a large number of design variables (Choi and Kim, 2004).

4.4. Convergence to the optimum

The optimization process is terminated whenever a convergence criterion is satisfied. The employed design optimization tool (DOT) uses several criteria to make the decision when to stop. These include a maximum number of iterations, "reasonable" satisfaction of the Kuhn–Tucker conditions and diminishing returns. These criteria are elaborated in Vanderplaats (1999) in details.

5. Numerical results and discussions

In order to demonstrate the abilities of the proposed method for material design of FGM structures, some numerical examples are here presented. We consider two-phase FGMs composed of a combination of Al_2O_3 and Ni which is regarded as an ideal candidate for thermo-mechanical applications by exploiting the heat resistance of the ceramic phase and fracture resistance of the metal one.

At the first model problem, we verify the presented results by optimization of a three layered Ni–Al_2O_3 FGM square plate for which the optimal results of other numerical methods such as finite elements (Cho and Ha, 2002b) and meshless method (Goupee and Vel, 2006b) are available in the literature. Next, we consider material distribution optimization of an FG infinite plate with hole under various mechanical and thermal loads. It needs to be mentioned that, in the following examples, the control weights of the material profiles are set to one, so the volume fraction NURBS surfaces degenerate to B-splines. Also, numerical integrations are performed by Gauss quadrature and using 9 Gauss points per knot element.

5.1. Model problem 1

As the first model problem, for the sake of verification of the obtained results, we address two-dimensional volume fraction optimization of a three layered FGM component which is also considered in many researches such as Cho and Ha (2002b) and Goupee and Vel (2006b), thus far. Fig. 1 shows the configuration of a half of a simply supported square plate which is intended to be comprised of a combination of Ni and Al_2O_3 with the material properties listed in Table 1.

Table 1
Material properties of Ni and Al_2O_3.

Property	E (GPa)	ν	α (10^{-6}/K)	k (W/mK)	ρ (kg/m^3)
Ni	199.5	0.30	15.4	60.7	8880
Al_2O_3	393.0	0.25	7.4	30.0	3960

As the figure shows, the symmetry condition is applied to the left edge of the plate. It is also observed that, the plate is made of two homogeneous layers of pure Ni and Al_2O_3 at the top and bottom edges, respectively, with a graded layer in the middle. The plate is assumed to be cooled to 300 K from an initial temperature of 1000 K. In this example, we attempt to minimize the peak effective thermal residual stress starting from a linearly graded layer. The computational model of the plate is depicted in Fig. 2. As the figure shows, we have employed a single patch constructed by a net of 14×12 control points for modeling and optimization of the FG plate. Instead of using multiple patches including two homogeneous and a graded one for modeling the initial material profile, we have increased the multiplicity of the appropriate knots that fall on $y = 0.01$ and $y = 0.09$ in the physical space. This provides us the possibility of creating the linear variation of the graded zone using a single patch exactly. Moreover, it is mentioned that we have used linear parameterization of computational domain and quadratic basis functions in both directions.

Denoting the volume fraction of the ceramic phase, i.e. Al_2O_3, by V_c, the present optimization problem is stated as

$$\text{Minimize } f(V_c^{(i,j)}) = \text{Max}(\overline{\sigma}),\ i = 1, 2, \ldots, n_1 \text{ and } j = 3, 4, \ldots, n_2 - 3, \tag{30}$$

where $V_c^{(i,j)}$ are the applicates of the control points that construct the ceramic volume fraction NURBS surface and are considered as the design variables. As the formulation shows, the applicates of the control points corresponding to the homogeneous layers are removed from the design space to preserve their material properties unchanged. Likewise, the applicates of the control points that fall on the left edge of the plate ($i = 0$) are also omitted from the design space to apply the symmetry conditions on this edge. These applicates are assigned the same values of their adjacent control pints

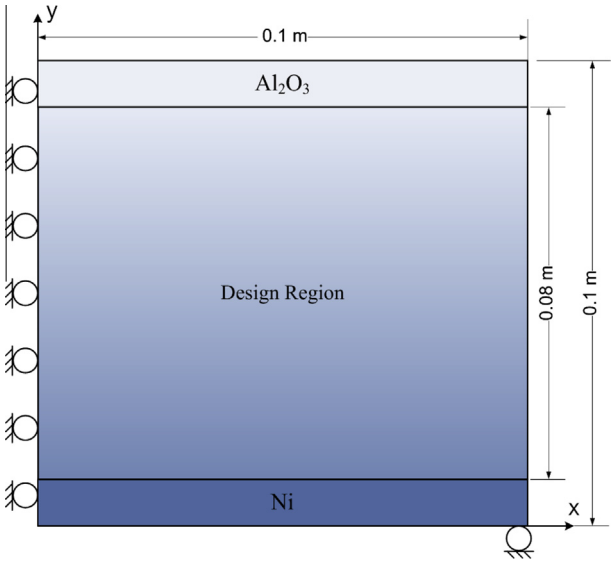

Fig. 1. Configuration of one half of the three-layered FG plate.

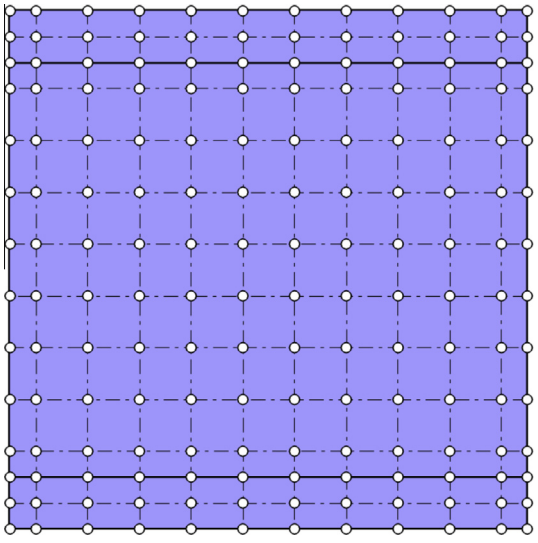

Fig. 2. Isogeometric computational model of the three-layered FG plate.

$(i = 1)$ to ensure C^1 continuity of the material profile throughout the graded zone of the whole plate.

For the sake of possibility of comparison of the obtained results, we use the same modified rule of mixtures as employed in Cho and Ha (2002b) and Goupee and Vel (2006b) for estimation of the effective material properties. The proposed modified rule of mixtures estimates the Young's modulus as follows (Tomota et al., 1976).

$$E = \frac{aV_mE_m + V_cE_c}{aV_m + V_c}, \quad a = \frac{q + E_c}{q + E_m} \tag{31}$$

As given in this equation, this estimate includes additional parameter q $(0 \leqslant q \leqslant +\infty)$ defined as the stress–strain transfer ratio. Considering Eq. (31), we observe that the choice of $q = +\infty$ is identical to the linear rule of mixtures. In addition, for any choice of q, E is bounded by the Young's moduli of two constituents. Since the appropriate value of q depends on the type of base materials, it should be determined numerically or/and experimentally for any specific FGM component (Cho and Ha, 2002b). According to the work of Cho and Ha (2000) by the finite element method, it has been found that the choice of 500 GPa for q is suitable for the spatially well-dispersed Ni–Al_2O_3 FGMs.

On the other hand, for the thermal expansion coefficient, by assuming the difference in thermal expansion coefficients of two base materials to be reasonably small, the Schapery's estimate (Schapery, 1968) is employed, wherein the averaged thermal expansion coefficient for dual-phase materials with arbitrary phase geometry is expressed as (Schapery, 1968)

$$\alpha = V_m\alpha_m + V_c\alpha_c - \frac{1/K_L - 1/\hat{K}}{1/K_m - 1/K_c}(\alpha_m - \alpha_c) \tag{32}$$

in which $1/K_L = V_m/K_m + V_c/K_c$, and $\hat{K}$ is the averaged bulk modulus of dual-phase graded materials. It is evident that in Eq. (32), the averaged thermal expansion coefficient depends on the choice of $\hat{K}$. Considering the research of Cho and Ha (2000), we observe that the Schapery's estimate leads to thermal stress distributions consistent well with those by the finite element discretized models, for a wide range of volume fractions, when $\hat{K}$ is predicted by the linear rule of mixtures. In this research, for the sake of consistency in the material model, the same modified rule of mixtures with $q = 500$ GPa used for the Young's modulus is adopted for the thermal conductivity.

The maximum effective stress of the initial model is 285.3 MPa, which is in good agreement with the peak effective stress reported by Goupee and Vel (2006b), that is 293.1 MPa and is obtained by the element free Galerkin (EFG) method.

The obtained optimal distribution of Al_2O_3 volume fraction is depicted in Fig. 3. The peak effective stress of the illustrated optimum distribution has decreased to 146.2 MPa which is equivalent to 48.8% reduction of initial one. It is also noted that the obtained optimum peak effective stress is much better than that reported by Cho and Ha (2002b) using the FEM, i.e. 268.5 MPa, and in good agreement with the result of Goupee and Vel (2006b) by the EFG method employing a grid of 4×6 points as the design variables and a genetic algorithm for optimization, i.e. 153.8 MPa. It is evident that the smoothness of the material profile is very crucial to decreasing the stress components. Following the previous mentioned fact regarding the order of continuity of NURBS surfaces, we realize that the obtained material distribution is at least C^1 continuous throughout the graded layer which, as Fig. 3 clearly shows, has resulted in a very smooth material profile.

The distributions of the effective stress in the initial and final designs are illustrated in Fig. 4. As Fig. 4(a) shows, the initial effective stress distribution contains an abrupt gradation to the peak stress near the top edge. On the other hand, as seen in Fig. 4(b), the optimum distribution dissipates this concentration throughout the structure so that decrease its peak value by nearly half.

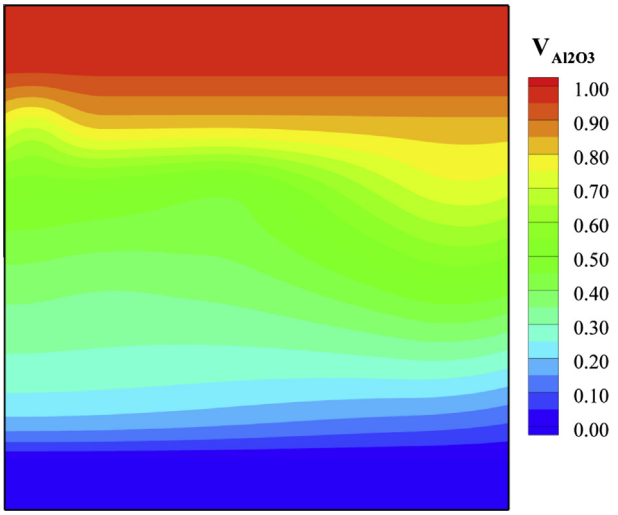

Fig. 3. Optimal distribution of Al_2O_3 volume fraction for minimization of the effective stress.

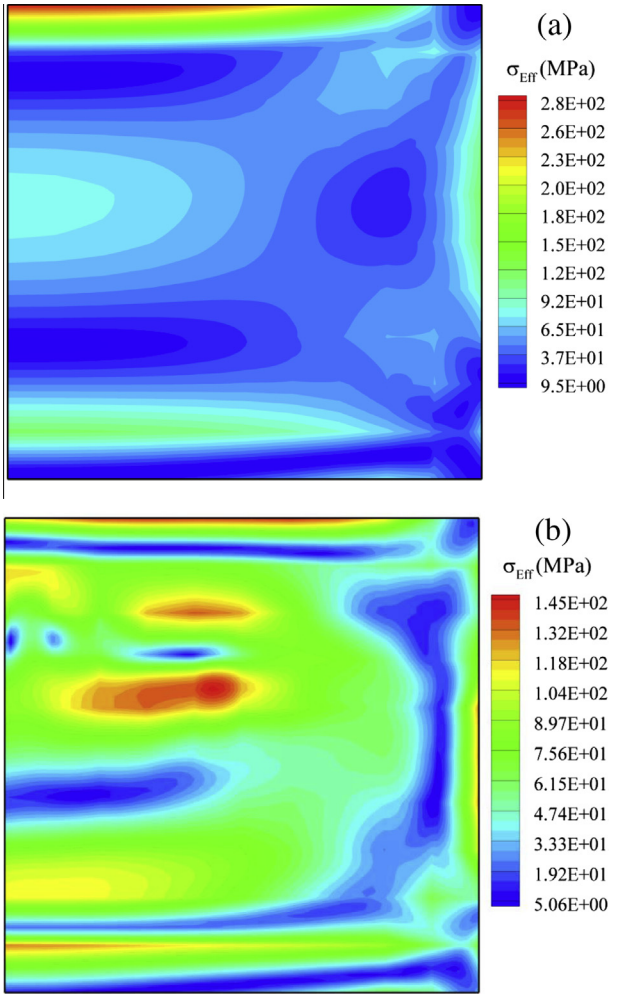

Fig. 4. Distribution of the effective stress in the (a) initial model and (b) final design.

The history of the objective function is demonstrated in Fig. 5. The figure shows that the peak effective stress abruptly decreases at the early iterations and the optimum is obtained after 10 iterations.

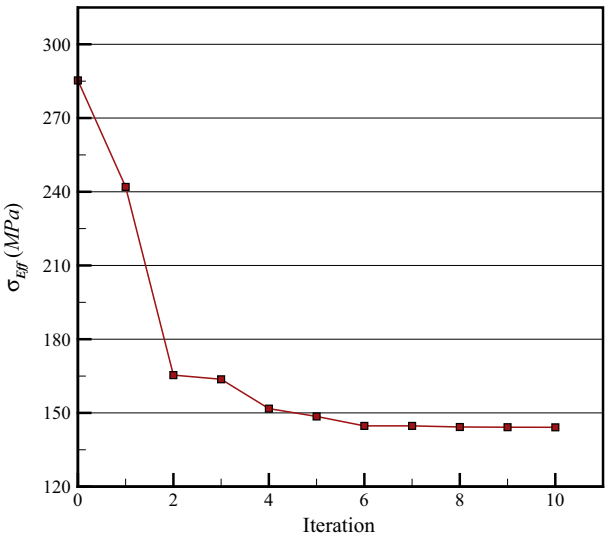

Fig. 5. The history of the objective function for minimization of the maximum effective stress.

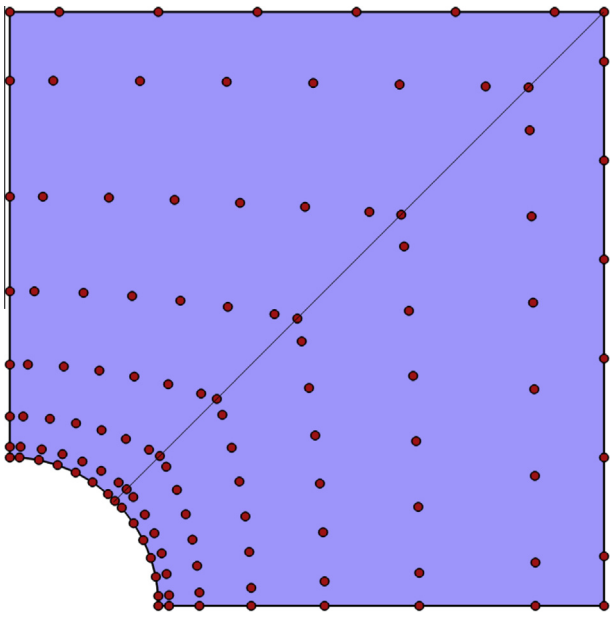

Fig. 7. The isogeometric computational model for simulation of the square plate with hole.

5.2. Model problem 2

As the next model problem, we consider an infinite plate with a circular hole under both mechanical and thermal loads. The infinite plate is modeled by a finite quarter plate with the configuration depicted in Fig. 6. As observed, the plate is subjected to a uniform traction applied to its right side and a uniform heat flux applied to its top side. Moreover, the left and right sides of the plate as well as the circular hole are assumed to be isolated ($q = 0$), while its bottom side is held at the reference temperature, that is $T(x, 0) = T_0$.

It is noted that the exact elasticity solution for the infinite homogeneous plate with a circular hole under uniform traction at infinity is available at Sadd (2009). Besides, the exact solution of the Laplace equation with the mentioned thermal boundary conditions for the homogeneous plate is taken from Sadd (2009) as

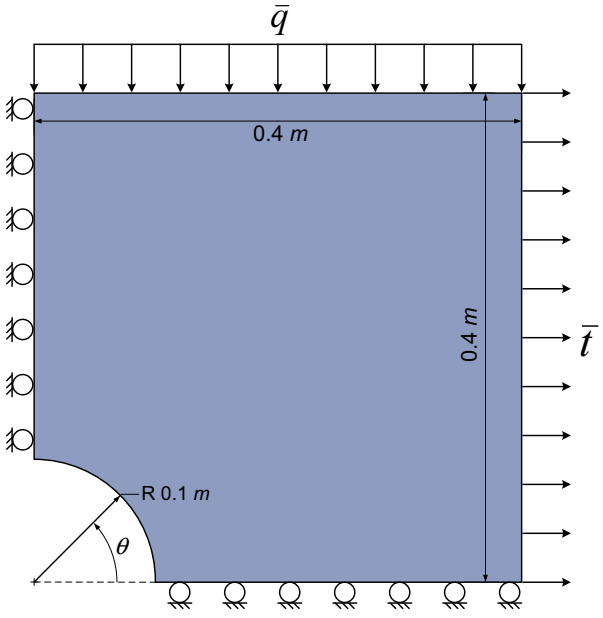

Fig. 6. Configuration and boundary conditions of the square plate with hole.

$$T(r,\theta) = \frac{\bar{q}}{k}\left(r + \frac{R^2}{r}\right)\sin(\theta) \tag{33}$$

where R is the radios of the circular hole.

The employed isogeometric computational model of the plate is represented in Fig. 7. As we know, different strategies are available for the construction of the geometry of this example using a single patch. The primary approach is repeating the control point which falls on the upper right corner of the plate. This ensures having C^1 continuity across all the interior element boundaries, but at the expense of having a singularity at the corner where the control point is repeated, as well as having an irregular mesh. An alternative strategy, which is also adopted here, is increasing the multiplicity of the middle knot of the respective knot vector (Ξ) by one. This brings about the possibility of having a regular mesh, but at the expense of losing an order of continuity of the solution and the material profile on the middle knot line, i.e. $\xi = 0.5$ which is highlighted in the figure.

As Fig. 7 demonstrates, we employ a net of 15×8 control points for simulation of the plate. Similar to previous example, in order to apply the symmetry conditions on the left and bottom edges of the plate and obtain a C^1 continuous material profile on these borders, the first and last set of control points corresponding to $i = 0$ and $i = n_1$ are removed from the design space and assigned the same applicates of their adjacent control points, that are $i = 1$ and $i = n_1 - 1$, respectively. In this example, we consider three cases with different loading conditions and optimization objectives. In all cases, the effective material properties are estimated by using the Mori–Tanaka scheme with Ni as the matrix.

As the first case, we assume $\bar{q} = 0$ and the plate is only subjected to a traction $\bar{t} = 100$ MPa. In this case, starting from a monolithic ceramic plate, we seek to find the optimum distributions of the constituents to minimize the peak value of the normal stress component σ_{xx}, without any optimization constraints. It is noted that under the assumed loading conditions, σ_{xx} is the major stress component. The peak value of this stress component for the homogeneous plate occurs at $r = 0.1$ and $\theta = \pi/2$ which equals 358 MPa. This is also in good agreement with the stress concentration factor

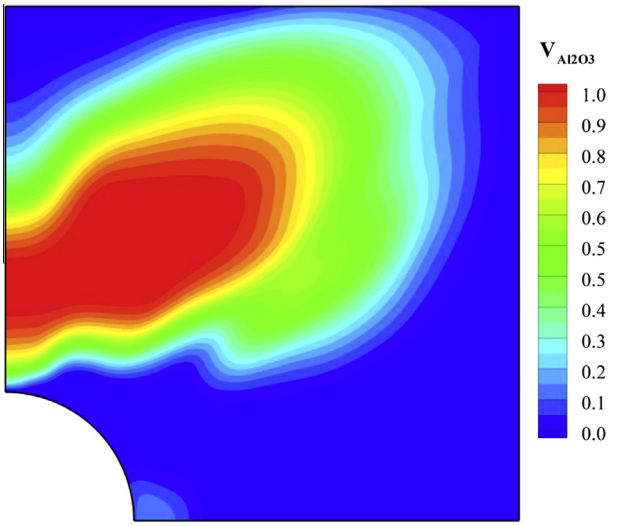

Fig. 8. Optimal distribution of Al_2O_3 for minimization of σ_{xx} under traction.

3 predicted by the exact elasticity solution (Sadd, 2009) for an infinite plate containing a circular hole under a tensile traction at infinity.

The optimization problem for this case is stated as

$$\text{Minimize } f(V_c^{(i,j)}) = \text{Max}(\sigma_{xx}), \quad i = 1,2,\ldots,n_1 - 1 \text{ and } j = 0,1,\ldots,n_2 \tag{34}$$

The optimum distribution of the ceramic phase volume fraction is demonstrated in Fig. 8. It is noted that during the optimization procedure, the contribution of the ceramic phase has decreased to 34% by volume. It is interesting to note that the peak value of this stress component is reduced by 45% during the optimization process and achieved 197 MPa in the final design. The obtained optimal distribution represented in Fig. 8 can be justified with regards to the stress distributions in the initial and final designs depicted in Figs. 9(a) and (b), respectively.

Considering the optimum distribution of the ceramic phase, we observe that the regions very near to the circular hole are comprised of pure metallic phase which, regarding to the presented properties in Table 1, has much lower stiffness compared to the ceramic one, that is roughly 1:2. It is evident that as a region is composed of a softer phase, sustains lower magnitude of the stress components. Hence, the optimization process moves the stiffer ceramic phase upward to lighten the stress concentration near the hole and takes the burden of sustaining the stress to its vicinity as clearly seen in Fig. 8. According to Fig. 9(b), this optimum distribution dissipates the stress concentration around the hole to its surroundings and in this way highly decreases its peak value.

The history of the objective function is also represented in Fig. 10. Due to the fact that in this case, there is no optimization constraint and the optimum distribution of the volume fractions is not too complex, it is seen that the optimum is found after a relatively small number of iterations with high reduction of the objective function at the early iterations.

As the next case, we address volume fraction optimization of the plate under only a uniform heat flux $\overline{q} = 100\ \text{kW/m}^2$. In this case, we attempt to find the optimum distribution of material constituents to minimize the peak effective stress so that the maximum temperature in the plate does not exceed a prescribed value of $\overline{T}_{\text{Max}} = 900\ \text{K}$. This optimization problem is mathematically stated as follows with the same design variables as the previous case.

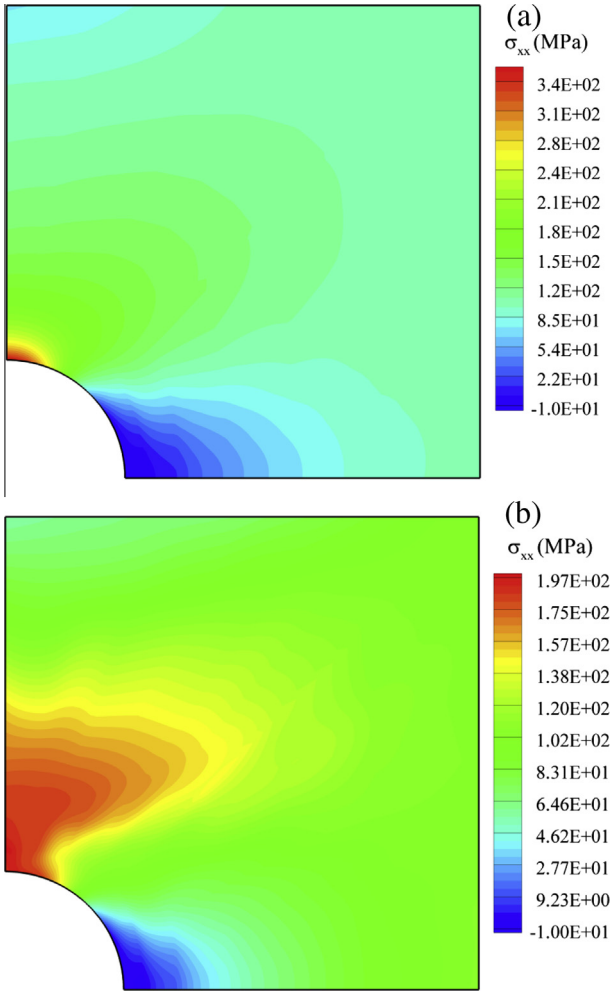

Fig. 9. Distribution of σ_{xx} under traction in the (a) initial and (b) optimum design.

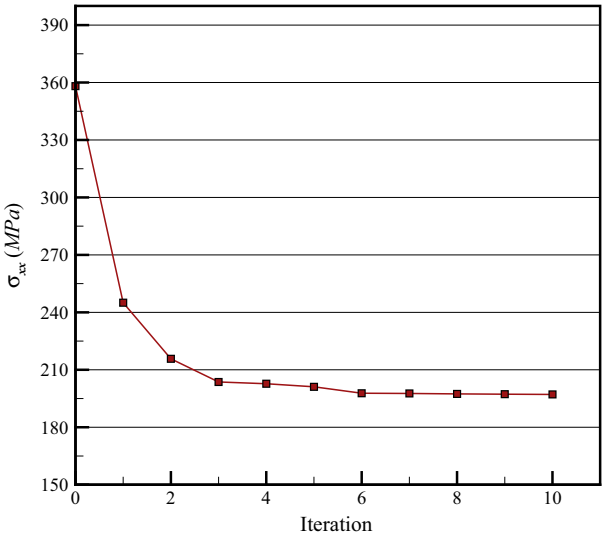

Fig. 10. The history of the objective function for minimization of σ_{xx} under traction.

$$\text{Minimize } f(V_c^{(i,j)}) = \text{Max}(\overline{\sigma})$$
$$\text{Subject to: } g_1(V_c^{(i,j)}) = \frac{1}{\overline{T}_{\text{Max}}}[\text{Max}(T)] - 1 \leqslant 0 \tag{35}$$

Table 2
The maximum temperature and effective stress in the homogeneous plates together with their total masses.

Material	T_{Max} (K)	$\overline{\sigma}_{Max}$ (GPa)	Mass (kg)
Al_2O_3	1497	1.958	602.5
Ni	740	1.021	1351.0

The maximum effective stress and temperature of the monolithic plates as well as their total masses are presented in Table 2 for comparison. In this case, we start the optimization process from a homogeneous metal plate which, according to Table 2, has a lower peak effective stress and also is a feasible model. The obtained optimum distribution of the ceramic phase comprised of 30.2% of this phase is represented in Fig. 11. The lower portion of the ceramic phase was also expected because, according to Table 1, Al_2O_3 has a much lower thermal conductivity than Ni. On the other hand, as Eq. (33) shows, the temperature value is proportional to the reciprocal of the thermal conductivity. Accordingly, since the applied temperature constraint is close to the maximum temperature occurs in the monolithic metal plate, it was predictable that the optimum to be more comprised of this phase in order to satisfy the applied constraint. It is interesting to note that the illustrated optimum distribution has decreased the peak effective stress to 594 MPa which is respectively 68.9% and 40.2% less than those of the homogeneous ceramic and metal plates. As observed, the optimum distribution contains a large region of the metallic phase around the hole, while it is rich of the ceramic phase nearby the right and top sides.

The effective stress distributions in the initial and final models are illustrated in Fig. 12. As the figure shows, the optimum volume fraction distribution has dissipated the stress concentration around the hole and at the lower right corner of the initial model so that it has highly relieved the peak effective stress value. Moreover, the maximum temperature of the optimum plate is 896 K which falls near the applied constraint and is more than 40% less than that of the monolithic ceramic plate. The history of the objective function for this case is represented in Fig. 13. As observed, in this case the optimum is found after 15 iterations. It is also seen that at the final iterations, no significant change in the objective function occurs; then DOT assumes the convergence and terminates the optimization process.

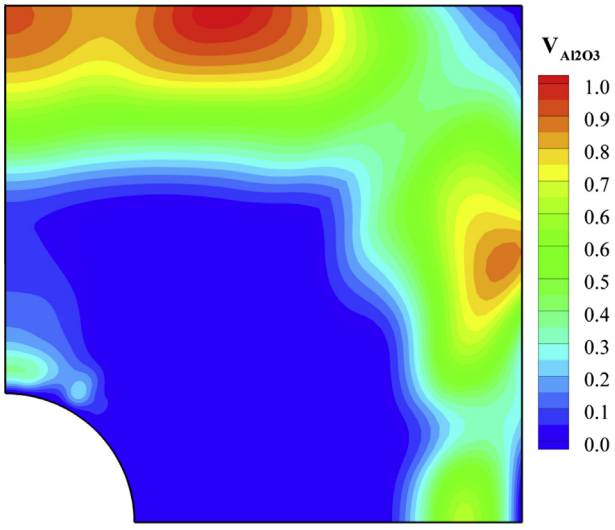

Fig. 11. Optimal distribution of Al_2O_3 volume fraction for minimization of the effective stress under heat flux.

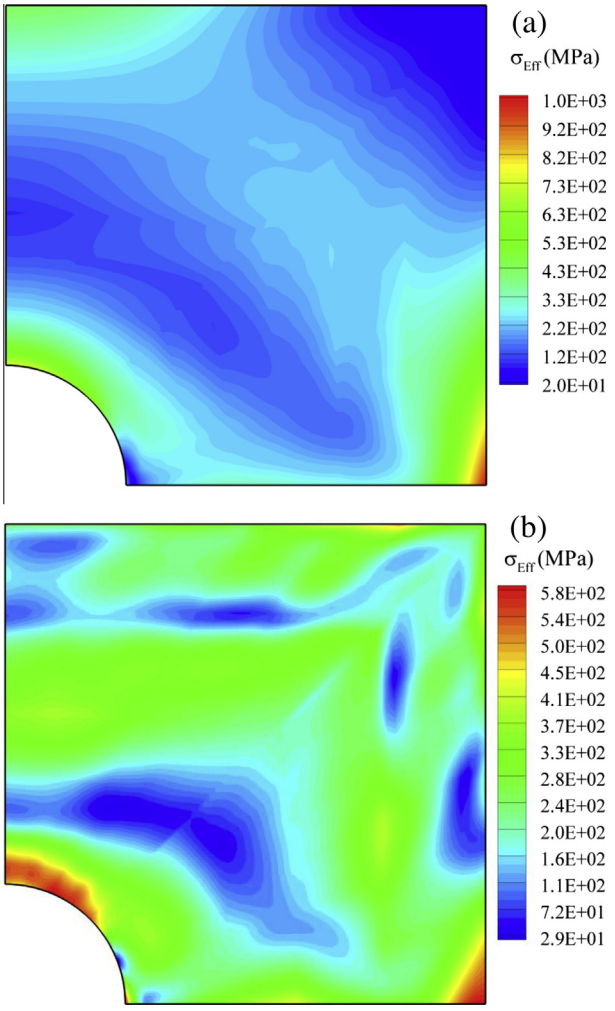

Fig. 12. Distribution of the effective stress in the (a) initial model and (b) final design.

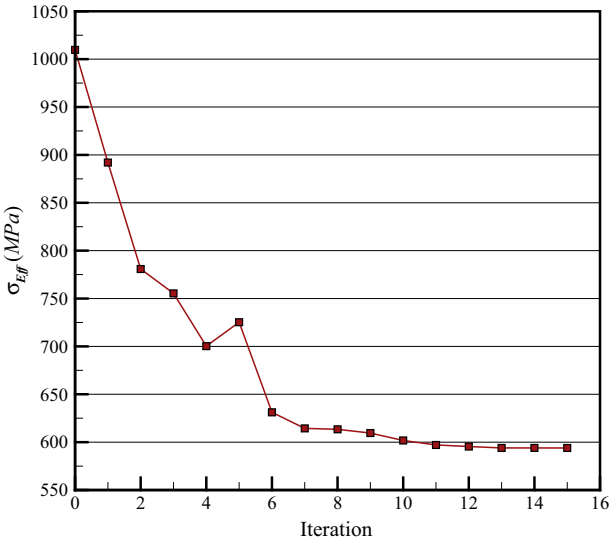

Fig. 13. The history of the objective function for minimization of the effective stress under heat flux.

The present case study demonstrated that the appropriate volume fraction distribution of the constituent phases can result in simultaneous stress and temperature reduction of the FG bodies

exposed to thermal loadings and considerably improve their thermo-mechanical performance.

Due to the fact that in many applications mass of the structure is of primary importance, as the final case we consider volume fraction optimization of the constituents to minimize the total mass of the plate. On the other hand, preventing the maximum effective stress and the maximum temperature experienced by the FGM components not to exceed prescribed values are usually essential concerns in designing FG structures. Hence, in this example, we prescribe the maximum effective allowable stress of $\overline{\sigma}_{\text{Max}} = 1$ GPa and the maximum allowable temperature of $\overline{T}_{\text{Max}} = 1000$ K. Consider the plate of Fig. 6 to be subjected to both traction and heat flux loadings $\overline{t} = 100$ MPa and $\overline{q} = 100$ kW/m^2. The peak effective stresses under this loading condition are 1.94 GPa and 1.10 GPa for the monolithic ceramic and metal plates, respectively. Starting from a monolithic ceramic plate, we seek to minimize the total mass of the plate with the mentioned prescribed constraints. The present optimization problem is stated as follows with the same design variables as previous cases.

$$\begin{aligned} &\text{Minimize } f(V_c^{(i,j)}) = \int_V (\rho_c V_c + \rho_m (1 - V_c)) dV \\ &\text{Subject to: } g_1(V_c^{(i,j)}) = \frac{1}{\overline{\sigma}_{\text{Max}}} [\text{Max}(\overline{\sigma})] - 1 \leqslant 0, \quad \text{and} \\ &\qquad\qquad g_2(V_c^{(i,j)}) = \frac{1}{\overline{T}_{\text{Max}}} [\text{Max}(T)] - 1 \leqslant 0 \end{aligned} \tag{36}$$

The obtained optimum distribution of the ceramic volume fraction in the plate is depicted in Fig. 14. The optimum distribution contains 53.7% of the ceramic phase and weighs 948.9 kg.

Due to applying different constraints to the present optimization problem, the detailed interpretation of the optimum distribution depicted in Fig. 14 is not as easily possible; however, contemplating the obtained volume fraction distribution with regards to the distribution of the effective stress in the initial and final designs represented in Fig. 15 brings us about the possibility of some justifications.

According to Table 1, Al_2O_3 has much lower density compared to the metallic Ni phase, so the initial design yields the lowest value of the objective function. However, the initial monolithic ceramic plate highly violates both the applied constraints of the peak effective stress and maximum temperature and makes it an infeasible material distribution. Therefore, the optimization process

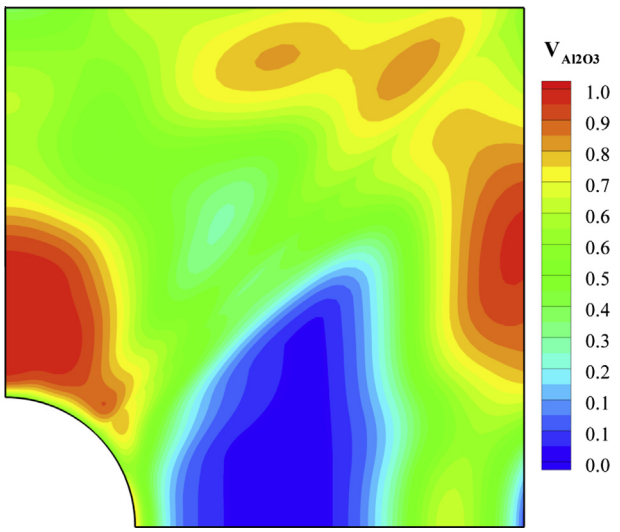

Fig. 14. Optimal distribution of Al_2O_3 volume fraction for mass minimization of the plate under simultaneous traction and heat flux.

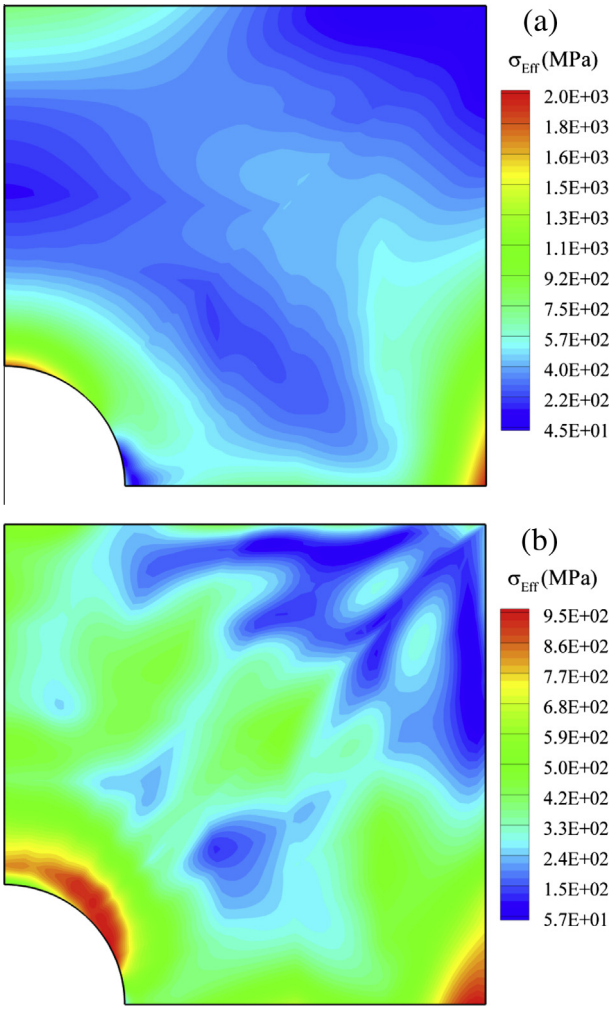

Fig. 15. Distribution of the effective stress in the (a) initial model and (b) final design.

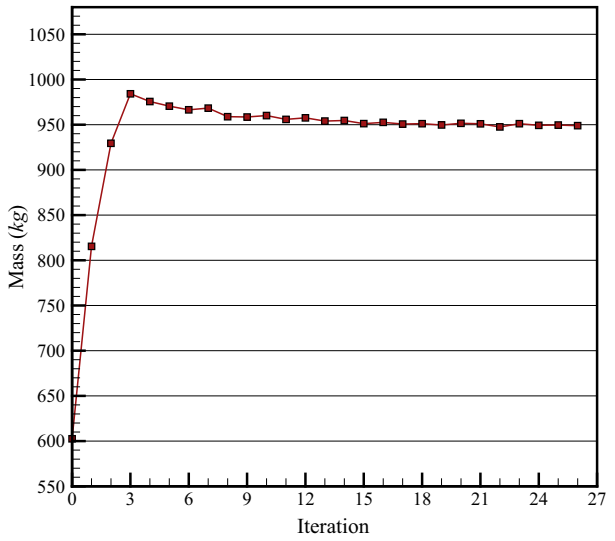

Fig. 16. The history of the objective function for mass minimization of the plate under simultaneous traction and heat flux.

attempts to move toward a feasible region, which, as observed in the history of the objective function plotted in Fig. 16, results in sharp increase of the objective function at the early iterations.

Fig. 14 shows that the optimum distribution contains regions rich of the stiffer ceramic phase on the left and right edges of the plate and a zone rich of the softer metallic phase at its bottom edge. According to depicted stress distribution in the final design, this volume fraction distribution dissipates the stress concentration of the initial model and declines it to the prescribed allowable value in a manner to contain the least possible volume ratio of the metallic phase. Doing this, results in an optimum that weighs 29.8% less than the homogeneous metal plate while satisfies both the applied constraints. Furthermore, it is seen that despite employing a relatively small numbers of control points, a very complex material profile is accomplished which demonstrates the high abilities of splines in creation of complicated shapes and surfaces. Due to the fact that the optimum volume fractions profiles for this case are more complex compared to the previous cases, as Fig. 16 shows, the optimum is acquired after a larger number of iterations.

Considering the optimization results of this case, we can see that, despite lightening the peak effective stress, the optimum design is much lighter that the monolithic metal plate. So, it is seen that suitable design of FGMs can result in simultaneously mass and stress reduction of structures and yield very desirable designs with high thermo-mechanical performance.

6. Conclusions

We developed a new methodology in the framework of isogeometric analysis for optimization of volume fraction distribution of functionally graded structures. In this approach, variations of the material constituents' volume fractions are constructed by imaginary NURBS surfaces in a fully isogeometric formulation using the same basis functions employed for construction of the geometry and approximation of the solution. As observed, owing to many significant properties of NURBS basis functions and surfaces such as the strong convex hull property and the ability of creating very complex material profiles employing quite a few numbers of control points, the proposed method circumvents the serious difficulties of the available methods efficiently. Moreover, these properties provide the accessibility of any desired order of continuity for the material distribution which consequently results in very smooth material profiles that are also easier to fabricate. A few numerical examples regarding volume fraction optimization of two phase Ni–Al_2O_3 FG structures presented and demonstrated the performance and capabilities of this method. As observed, the appropriate distribution of material constituents in FGMs can effectively improve the thermo-mechanical performance of these structures. It was shown that, suitable material distribution of FGMs can result in decreasing the peak effective stress or the peak temperature experienced by the structure even by simultaneous reduction of the structural mass which is very desirable in many engineering applications. The proposed method can also be easily extended to 3D elasticity problems or FGMs with more than two constituent phases.

Acknowledgements

The support from grant provided by the Ferdowsi University of Mashhad is gratefully acknowledged.

References

Almeida, S.R.M., Paulino, G.H., Silva, E.C.N., 2010. Layout and material gradation in topology optimization of functionally graded structures: a global–local approach. Structural and Multidisciplinary Optimization 42, 855–868.

Bobaru, F., 2007. Designing optimal volume fractions for functionally graded materials with temperature-dependent material properties. Journal of Applied Mechanics 74, 861–874.

Boussaa, D., 2009. Optimization of temperature-dependent functionally graded material bodies. Computer Methods in Applied Mechanics and Engineering 198, 2827–2838.

Brodlie, K., Mashwama, P., Butt, S., 1995. Visualization of surface data to preserve positivity and other simple constraints. Computers & Graphics 19, 585–594.

Chareonsuk, J., Vessakosol, P., 2011. Numerical solutions for functionally graded solids under thermal and mechanical loads using a high-order control volume finite element method. Applied Thermal Engineering 31, 213–227.

Chiba, R., Sugano, Y., 2012. Optimisation of material composition of functionally graded materials based on multiscale thermoelastic analysis. Acta Mechanica 223, 891–909.

Ching, H., Yen, S., 2005. Meshless local Petrov-Galerkin analysis for 2D functionally graded elastic solids under mechanical and thermal loads. Composites Part B: Engineering 36, 223–240.

Cho, J.R., Ha, D.Y., 2000. Averaging and finite-element discretization approaches in the numerical analysis of functionally graded materials. Materials Science and Engineering A 302, 187–196.

Cho, J.R., Ha, D.Y., 2002a. Volume fraction optimization for minimizing thermal stress in Ni–Al_2O_3 functionally graded materials. Materials Science and Engineering A 334, 147–155.

Cho, J.R., Ha, D.Y., 2002b. Optimal tailoring of 2D volume-fraction distributions for heat-resisting functionally graded materials using FDM. Computer Methods in Applied Mechanics and Engineering 191, 3195–3211.

Choi, K.K., Kim, N.H., 2004. Structural Sensitivity Analysis and Optimization 1: Linear Systems. Springer.

Ding, H.J., Huang, D.J., Chen, W.Q., 2007. Elasticity solutions for plane anisotropic functionally graded beams. International Journal of Solids and Structures 44, 176–196.

Embar, A., Dolbow, J., Harari, I., 2010. Imposing Dirichlet boundary conditions with Nitsche's method and spline-based finite elements. International Journal for Numerical Methods in Engineering 83, 877–898.

Feng, Y., Jin, Z., 2009. Thermal fracture of functionally graded plate with parallel surface cracks. Acta Mechanica Solida Sinica 22, 453–464.

Goupee, A.J., Vel, S.S., 2006a. Optimization of natural frequencies of bidirectional functionally graded beams. Structural and Multidisciplinary Optimization 32, 473–484.

Goupee, A.J., Vel, S.S., 2006b. Two-dimensional optimization of material composition of functionally graded materials using meshless analyses and a genetic algorithm. Computer Methods in Applied Mechanics and Engineering 195, 5926–5948.

Goupee, A.J., Vel, S.S., 2007. Multi-objective optimization of functionally graded materials with temperature-dependent material properties. Materials & Design 28, 1861–1879.

Guo, L.C., Noda, N., 2010. An analytical method for thermal stresses of a functionally graded material cylindrical shell under a thermal shock. Acta Mechanica 214, 71–78.

Guo, L.C., Noda, N., Wu, L., 2008. Thermal fracture model for a functionally graded plate with a crack normal to the surfaces and arbitrary thermomechanical properties. Composites Science and Technology 68, 1034–1041.

Hassani, B., Taheri, A.H., Moghaddam, N.Z., 2013. An improved isogeometrical analysis approach to functionally graded plane elasticity problems. Applied mathematical modelling 37, 9174–9190.

Hill, R., 1965. A self-consistent mechanics of composite materials. Journal of the Mechanics and Physics of Solids 13, 213–222.

Hughes, T.J.R., Cottrell, J.A., Bazilevs, Y., 2005. Isogeometric analysis: CAD, finite elements, NURBS, exact geometry and mesh refinement. Computer Methods in Applied Mechanics and Engineering 194, 4135–4195.

Kim, J.-H., Paulino, G.H., 2002. Isoparametric graded finite elements for nonhomogeneous isotropic and orthotropic materials. Journal of Applied Mechanics 69, 502–514.

Kou, X.Y., Parks, G.T., Tan, S.T., 2012. Optimal design of functionally graded materials using a procedural model and particle swarm optimization. Computer-Aided Design 44, 300–310.

Kumar, A.V., Gossard, D.C., 1996. Synthesis of optimal shape and topology of structures. Journal of Mechanical Design 118, 68–74.

Liu, D.Y., Wang, C.Y., Chen, W.Q., 2010. Free vibration of FGM plates with in-plane material inhomogeneity. Composite Structures 92, 1047–1051.

Lü, C., Chen, W., Zhong, Z., 2006. Two-dimensional thermoelasticity solution for functionally graded thick beams. Science in China Series G: Physics, Mechanics and Astronomy 49, 451–460.

Lü, C.F., Chen, W.Q., Xu, R.Q., Lim, C.W., 2008. Semi-analytical elasticity solutions for bi-directional functionally graded beams. International Journal of Solids and Structures 45, 258–275.

Matsui, K., Terada, K., 2004. Continuous approximation of material distribution for topology optimization. International Journal for Numerical Methods in Engineering 59, 1925–1944.

Mori, T., Tanaka, K., 1973. Average stress in matrix and average energy of materials with misftting inclusions. Acta Metallica 21, 571–574.

Na, K.-S., Kim, J.-H., 2009a. Optimization of volume fractions for functionally graded panels considering stress and critical temperature. Composite Structures 89, 509–516.

Na, K.-S., Kim, J.-H., 2009b. Volume fraction optimization of functionally graded composite panels for stress reduction and critical temperature. Finite Elements in Analysis and Design 45, 845–851.
Na, K.-S., Kim, J.-H., 2010. Volume fraction optimization for step-formed functionally graded plates considering stress and critical temperature. Composite Structures 92, 1283–1290.
Nemat-Alla, M., 2009. Reduction of thermal stresses by composition optimization of two-dimensional functionally graded materials. Acta Mechanica 208, 147–161.
Paulino, G.H., Silva, E.C.N., 2005. Design of functionally graded structures using topology optimization. Materials Science Forum 492–493, 435–440.
Paulino, G.H., Silva, E.C.N., Le, C.H., 2008. Optimal design of periodic functionally graded composites with prescribed properties. Structural and Multidisciplinary Optimization 38, 469–489.
Piegl, L.A., Tiller, W., 1997. The NURBS Book. Springer-Verlag.
Sadd, M.H., 2009. Elasticity: Theory, Applications and Numerics. Academic Press.
Schapery, R.A., 1968. Thermal expansion coefficients of composite materials based on energy principles. Journal of Composite Materials 2, 380–404.
Sheng, G.G., Wang, X., 2011. Non-linear response of functionally graded cylindrical shells under mechanical and thermal loads. Journal of Thermal Stresses 34, 1105–1118.
Shiota, I., Miyamoto, Y., 1997. Functionally Graded Materials 1996. Elsevier Science.
Sinha, S.M., 2005. Mathematical Programming: Theory and Methods. Elsevier.
Spillers, W.R., Macbain, K.M., 2009. Structural Optimization. Springer, New York, USA.
Surendranath, H., Bruck, H.A., Gowrisankaran, S., 2003. Enhancing the optimization of material distributions in composite structures using gradient architectures. International Journal of Solids and Structures 40, 2999–3020.
Tomota, Y., Kuroki, K., Mori, T., Tamura, I., 1976. Tensile deformation of two-ductile-phase alloys: flow curves of $\alpha \rightarrow \gamma$ Fe–Cr–Ni alloys. Materials Science and Engineering 24, 85–94.
Turteltaub, S., 2002. Optimal control and optimization of functionally graded materials for thermomechanical processes. International Journal of Solids and Structures 39, 3175–3197.
Ueda, S., 2001. Thermal shock fracture in a W–Cu divertor plate with a functionally graded nonhomogeneous interface. Journal of Thermal Stresses 24, 1021–1041.
Valizadeh, N., Natarajan, S., Gonzalez-Estrada, O.A., Rabczuk, T., Bui, T.Q., Bordas, S.P.A., 2013. NURBS-based finite element analysis of functionally graded plates: static bending, vibration, buckling and flutter. Composite Structures 99, 309–326.
Vanderplaats, 1999. DOT – Design Optimization Tools, Users Manual, Version 5. Vanderplaats Research & Development, Inc., Colorado Springs, CO.
Wang, H., Qin, Q.-H., 2008. Meshless approach for thermo-mechanical analysis of functionally graded materials. Engineering Analysis with Boundary Elements 32, 704–712.
Xia, Q., Wang, M.Y., 2008. Simultaneous optimization of the material properties and the topology of functionally graded structures. Computer-Aided Design 40, 660–675.